

## Original article

# Dynamic behavior of droplet formation in dripping mode of capillary flow focusing

Ting Si<sup>✉\*</sup>

Department of Modern Mechanics, University of Science and Technology of China, Hefei 230027, P. R. China

### Keywords:

Flow focusing  
dripping mode  
droplet formation  
coalescence

### Cited as:

Si, T. Dynamic behavior of droplet formation in dripping mode of capillary flow focusing. *Capillarity*, 2021, 4(3): 45-49, doi: 10.46690/capi.2021.03.01

### Abstract:

Experimental study on the liquid dripping in a capillary flow focusing process is performed. Due to the high-speed gas stream that drives the inner liquid co-flowing through an orifice, complex phenomena for the droplet formation in dripping regime can be found as the gas pressure drop and the liquid flow rate change. Periodic dripping mode can produce uniform droplets, and non-periodic ones can result in satellites and droplets of different diameters. The droplet-droplet coalescence in the core of co-flowing gas stream is also obtained. The size of resultant droplets is measured under different values of gas pressure drop and liquid flow rate. It can be seen that the droplet size tends to decrease as the gas pressure drop increases and keeps nearly the same as the liquid flow rate increases. The results also indicate that the dynamic behavior of droplet formation in dripping mode of capillary flow focusing is mainly dominated by the gas pressure drop, and the capillary flow focusing technique can produce droplets with high throughput even in the dripping regime.

## 1. Introduction

Fine and controllable droplets are increasingly attractive because of their diverse scientific and engineering applications involving medicine, biology, chemistry, industry and agriculture. A number of droplet fabrication methods have been developed based on physical, chemical and physiochemical principles, in which microfluidic devices have been widely used in various applications (Stone et al., 2017; Zhu and Wang, 2017; Sohrabi et al., 2020). However, the formation of droplets with uniform size and high throughput is still a great challenge. In recent years, some top-down methods in terms of capillary flows have been demonstrated capable of stretching out fluid interfaces smoothly and steadily, resulting in monodisperse droplets (Barrero and Loscertales, 2007; Anna, 2016; Guerrero et al., 2020). One typical flow of them is the so-called capillary flow focusing (CFF), where surface tension stresses are overcome by hydrodynamic forces, characterized by the formation of a meniscus with tiny liquid volume emitted from its tip and focused in the core of a high-speed co-flowing gas stream through a small orifice (Gañán-Calvo, 1998).

In CFF, monodisperse droplets mainly result from axisym-

metric disturbances due to the Rayleigh instability, and the flows are usually classified as jetting and dripping which are closely related to the onset of convective instability and absolute instability, respectively (Si et al., 2009, 2010). The jetting mode keeps dominant in a wide range of parameters as the interfacial shear plays a significant role in retarding the Rayleigh instability, which has been widely studied previously (Evangeliio et al., 2016; Montanero and Gañán-Calvo, 2020). In the phase diagram of CFF, the liquid dripping can be found in a narrow range of Reynolds and Weber numbers (Si et al., 2009, 2010). The dynamic behaviors of dripping in liquid-driven CFF were reported recently (Mu et al., 2019), but those in gas-driven CFF haven't been studied thoroughly. It is still desirable to explore the dynamic behavior of liquid dripping and the movement of resultant droplets focused by co-flowing gas stream.

In this work, we mainly focus on the dripping mode in gas-driven CFF under different conditions. Three types of liquids with different physical properties are used as the inner liquid phase in experiments. The dynamic behavior of liquid dripping is described, and the size of resultant droplets as a function of

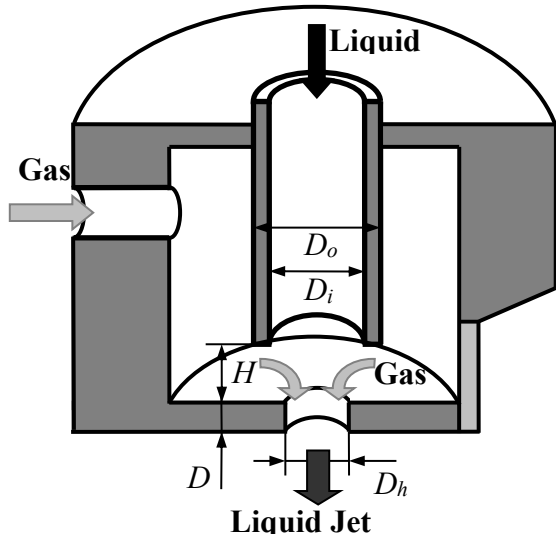


Fig. 1. Sketch of the CFF device.

mainly controllable parameters is obtained. The paper is organized as follows. First, the experimental methods are described, including the CFF device, the flow diagnostics and the materials. Second, the transition from jetting to dripping in CFF is obtained and the morphology of droplets in dripping mode is discussed for different liquids. Third, the movement of droplets in the core of surrounding gas stream is captured by high-speed video camera. The size of resultant droplets is measured under different values of gas pressure drop and liquid flow rate. Moreover, the droplet-droplet coalescence is also given. Finally, main conclusions are drawn.

## 2. Experimental methods

The assembled CFF chamber is sketched in Fig. 1. An orifice of diameter  $D_h$  is made in the center of the bottom wall of thickness  $D$ . The capillary tube of outer diameter  $D_o$  and inner diameter  $D_i$  enters through the top wall with an offset distance  $H$  from the mouth of the capillary tube to the orifice. The chosen geometric parameters are fixed in experiments, i.e.,  $D_i = 700 \mu\text{m}$ ,  $D_o = 900 \mu\text{m}$ ,  $D_h = 320 \mu\text{m}$ ,  $D = 900 \mu\text{m}$  and  $H = 820 \mu\text{m}$  (in Figs. 2 and 3), and  $D_i = 440 \mu\text{m}$ ,  $D_o = 640 \mu\text{m}$ ,  $D_h = 470 \mu\text{m}$ ,  $D = 200 \mu\text{m}$  and  $H = 560 \mu\text{m}$  (in Figs. 4-6), respectively. A quadrate cavity of area  $7 \times 5 \text{ mm}^2$  covered by an optical window perpendicular to the bottom wall is used to observe the whole process of the liquid flow from the position of the capillary tube to the droplet movement in the downstream. The capillary tube is adjusted to be coaxial with the orifice, and both the mouth of the capillary tube and the inner edge of the orifice are rounded to minimize the influence of undesirable disturbances. In experiments, the focused liquids mainly used are tap water, transformer oil and alcohol whose physical properties are given in Table 1 and the focusing gas is always air with  $\mu_2 = 1.79 \times 10^{-5} \text{ Pa}\cdot\text{s}$ ,  $\rho_2 = 1.25 \text{ kg/m}^3$  at  $T = 20 \text{ }^\circ\text{C}$ . The liquid with the flow rate of  $Q_l$  is supplied from the capillary tube by the syringe pump (WK-101P, China). The gas is forced by the gas storage through the side wall and the pressure drop between the inside

Table 1. Physical properties of experimental liquids.

Liquid	$\rho_1 (\text{kg/m}^3)$	$\mu_1 (\text{Pa}\cdot\text{s})$	$\rho (\text{N/m})$
Tap water	998.2	$1.00 \times 10^{-3}$	$7.30 \times 10^{-3}$
Transformer oil	877.5	$5.53 \times 10^{-3}$	$4.43 \times 10^{-3}$
Alcohol	789.4	$2.20 \times 10^{-3}$	$2.30 \times 10^{-3}$

and outside of the CFF device  $\Delta p_g$  is measured with the precise manometer.

The process of CFF begins with the formation of a drop attached to the orifice of the capillary tube that develops into a meniscus under the force of annular co-flowing air stream. In experiments, a high-speed video camera (FASCAM-SA5, Japan) illuminated with a continuous white light is used to capture the images. The movement and morphology of droplets can be observed continuously with a high time resolution. Besides, in order to capture the whole images of the flow with a high spatial resolution, we also use a microscope (SZ-B2/T2) combined with a charge coupled device camera (MTV-1802CB) illuminated with a stroboscopic lamp (PS-01A/B, with flash frequency in range of 50 to 12,000 Hz) and a large Fresnel lens (with the focus 127 mm) placed between the lamp and the CFF device. The stroboscopic lamp emits light in pulse with concentrated intensity and instantaneous images of the liquid dynamic behaviors can be clearly captured.

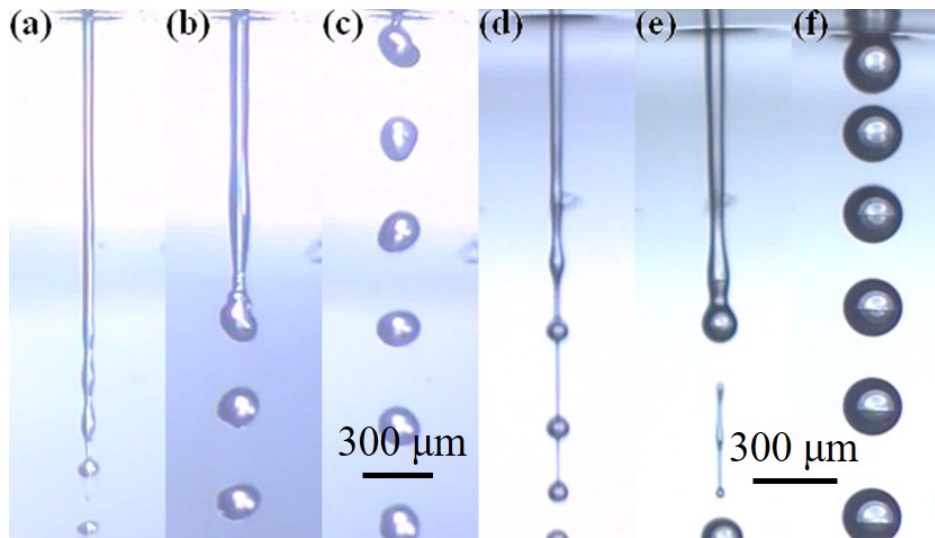
## 3. Results and discussion

Fig. 2 presents the typical photographs in the process of jetting-dripping (J-D) transition. For relatively high  $\Delta p_g$ , the liquid jet extends over distances of several times to the jet diameter. As the value of  $\Delta p_g$  is decreased, the unbroken jet is sharply shortened and the liquid dripping happens. Because of different physical properties of liquids, the critical values of  $\Delta p_g$  of the J-D transition for different cases are of great difference. It should be mentioned that there is a significant hysteresis effect in the process. Table 2 gives some critical values of  $\Delta p_g$  for J-D and D-J transitions in experiments. It can be seen that the critical values of  $\Delta p_g$  for J-D transition are much higher than those in reverse when the other parameters keep constant. The hysteresis effect is mainly caused by the global stability of the flow from the pressurized chamber up to the coaxial liquid-gas jets.

It is also seen from Fig. 2 that the droplet morphologies of transformer oil exhibit more uniform than those of tap water. In order to understand the principle, we introduce the Ohnesorge number (Oh) defined as the ratio between two characteristic times: the breaking time  $t_b$  and the viscous time  $t_v$ , which are given by,

$$t_b \sim (\rho_1 d_1^3 / \sigma)^{1/2} \quad \text{and} \quad t_v \sim \rho_1 d_1^2 / \mu_1 \quad (1)$$

where  $d_1$  is the diameter of the droplets. The breaking time  $t_b$  reflects the propagation of perturbations on the jet surface under the capillary force, and the viscous time  $t_v$  reflects the propagation of perturbations on the jet surface inside by viscous diffusion. Then Oh can be written as,



**Fig. 2.** Photographs in the J-D transition process. (a-c) Tap water,  $Q_l = 80$  ml/h,  $\Delta p_g = 5, 1.16, 1$  kPa and (d-f) transformer oil,  $Q_l = 40$  ml/h,  $\Delta p_g = 1, 0.5, 0.45$  kPa, sequentially.

**Table 2.** Critical values of  $\Delta p_g$  for J-D and D-J transitions (unit: Pa).

	Tap water			Alcohol			Transformer oil	
	40	60	80	40	60	80	40	60
J-D	1520	1145	968	278	227	193	380	298
D-J	1190	918	760	231	180	154	300	256

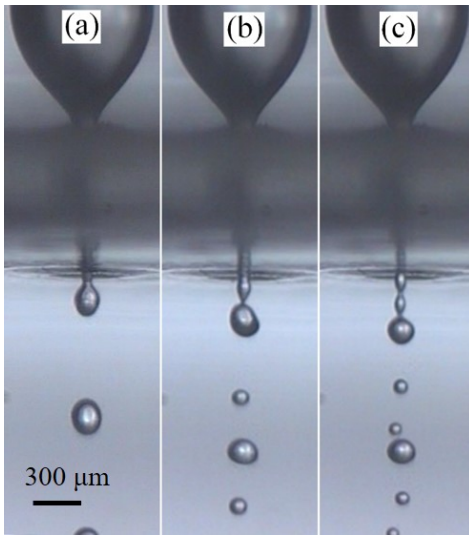


**Fig. 3.** Photographs of cone and droplets in dripping mode with tap water at  $Q_l = 80$  ml/h. (a)  $\Delta p_g = 1.13$  kPa; (b)  $\Delta p_g = 0.72$  kPa; (c)  $\Delta p_g = 0.96$  kPa.

$$\text{Oh} = \frac{\mu_1}{(\rho_1 d_1 \sigma)^{1/2}} \quad (2)$$

The value of Oh predicts the relative importance of viscosity on the jet breakup. If the diameters of droplets between different fluids are comparable (e.g.,  $d_1 = 400 \mu\text{m}$ ), It can be obtained that the value of Oh for transformer oil (i.e., about 0.14) is much larger than that for tap water (i.e., about

$5.9 \times 10^{-3}$ ). The viscosity of transformer oil plays a more significant role during the process of droplet formation. As a result, the droplets of transformer oil emitted from the tip of the meniscus have a spherical shape, while the water droplets are still non-spherical moving downstream.

In CFF experiments, different phenomena of liquid dripping can be observed owing to the specific CFF device and the force of co-flowing gas stream. Fig. 3 shows three typical photographs of meniscus and droplets with tap water for given geometric parameters. In addition to the uniform droplets, one or two satellites of much smaller diameters occasionally emerge between the neighboring main droplets. This interesting phenomenon may be attributed to the nonlinear dynamics of the flow in CFF, similar to the liquid-driven CFF cases (Mu et al., 2019). However, these phenomena seem to appear strongly dependent on the initial operation conditions. How to control the number of satellites is still unclear, which needs to be studied in the future.

As the external parameters are continuously adjusted in experiments, some regular rules can be obtained. Fig. 4 presents some photographs of droplet formation, indicating that as the value of  $\Delta p_g$  increases, the droplets are of one or two or sometimes three diameters alternately. It should be pointed out that the periodic and non-periodic droplet formation patterns can be observed alternatively. The distance between two neighboring droplets are different as the flow pattern changes. In a whole the diameter becomes smaller and smaller as  $\Delta p_g$  increases. The same tendency for other liquids can be also obtained in experiments.

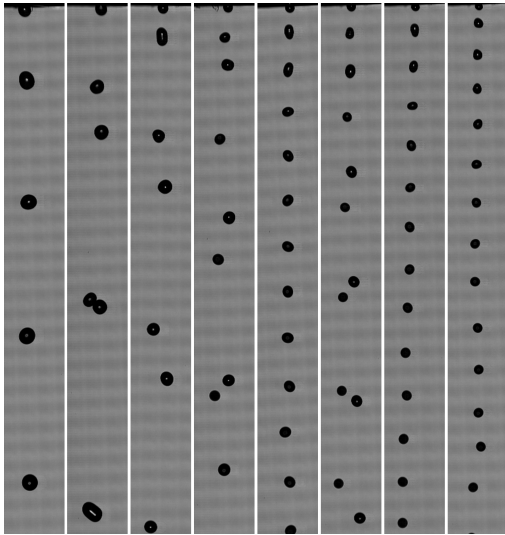


**Fig. 4.** Photographs of droplets with tap water at  $Q_l = 80$  ml/h.  $\Delta p_g = 448, 519, 626, 700, 770, 826, 926, 960$  Pa from left to right, sequentially.

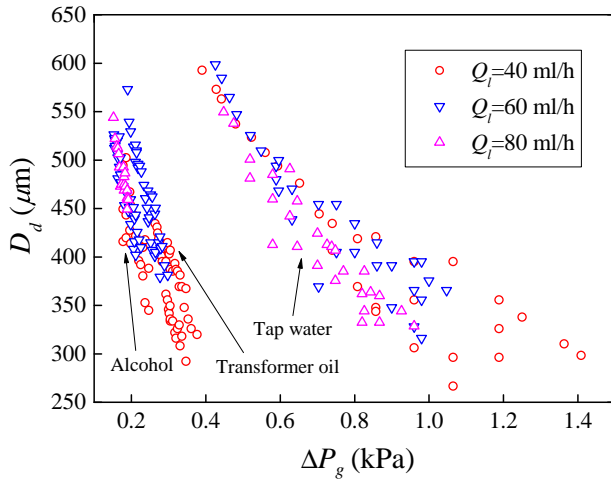


**Fig. 5.** The measured diameter of droplets versus  $\Delta p_g$  and  $Q_l$ .

In order to obtain the droplet size and its distribution quantitatively, the variation of measured diameter versus  $\Delta p_g$  and  $Q_l$  in the dripping regime is plotted in Fig. 5. In order to minimize the evaporation effect, the size of droplets is measured as soon as the droplets are collected from the downstream of the flow after the liquid jet breaks up. As  $\Delta p_g$  increases, the diameter tends to decrease, and as  $Q_l$  increases, the diameter keeps approximately constant. The reason lies in the fact that  $\Delta p_g$  is the energy of driving source and can be associated to the momentum of the focusing gas stream, while  $Q_l$  is just related to the focused liquid. Furthermore, the droplets for different liquids have nearly the same size distribution although the corresponding parametric ranges are distinct.

In experiments, the droplet-droplet coalescence is also observed. The detailed evolution in liquid dripping of CFF with a time interval of  $50 \mu\text{s}$  is shown in Fig. 6. The coalescent droplet first varies in shape and rotates continuously in the co-

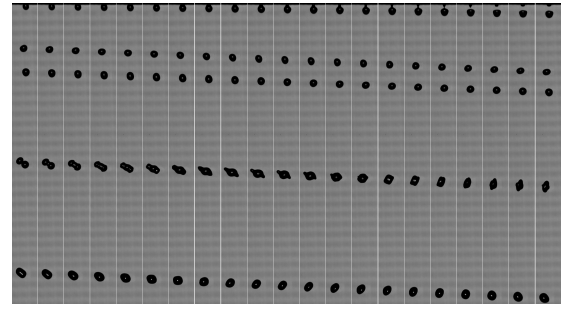


**Fig. 6.** The evolution of droplet-droplet coalescence in liquid dripping of CFF. The time interval is  $50 \mu\text{s}$ .

flowing gas stream. Sequentially, the collision results in configurations with a couple of spikes. The droplet eventually turns into a ball. The process is interesting and involves significant physical problems which call for detailed study in the future work.

Finally, it must be pointed out that the CFF technique is highly efficient in producing droplets even in the dripping regime. The production rate is easily deduced by,

$$f_d = \frac{6Q_l}{\pi d_1^3} \quad (3)$$

Taking  $Q_l = 80$  ml/h and  $d_1 = 400 \mu\text{m}$  for example, the number of droplets produced can be up to 663 per second. Furthermore, the gentle operating conditions motivate to replicate the CFF configuration into a multi-orifice structure, which will be valuable in various industrial applications.

#### 4. Conclusions and perspectives

The dynamic behavior of dripping in the CFF process has been performed experimentally. Different phenomena of liquid dripping are observed and the diameters of droplets are measured for different liquids. The gas pressure drop  $\Delta p_g$  is the main factor that affects the movement and morphology of droplets. Satellites, droplets of different diameters as well as perfectly monodisperse droplets are obtained in the dripping regime. The droplet-droplet coalescence is also observed. It can be seen that the CFF is a simple but efficient technique for producing droplets at high throughput. However, this work is still preliminary, and more studies should be performed in the future. The detailed analysis should be carried out to explore the physical mechanisms of the phenomena obtained in this work, and both the jetting and dripping modes should be studied thoroughly in order to provide guidance for practical applications.

#### Acknowledgement

This work was supported by the Youth Innovation Promotion Association CAS (No. 2018491), the Strategic Priority Research Program of the Chinese Academy of Sciences (No. XDB22040103) and the Fundamental Research Funds for the Central Universities.

#### Conflict of interest

The authors declare no competing interest.

**Open Access** This article is distributed under the terms and conditions of the Creative Commons Attribution (CC BY-NC-ND) license, which permits unrestricted use, distribution, and reproduction in any medium, provided the original work is properly cited.

## References

- Anna, S. L. Droplets and bubbles in microfluidic devices. *Annual Review of Fluid Mechanics*, 2016, 48: 285-309.
- Barrero, A., Loscertales, I. G. Micro- and nanoparticles via capillary flows. *Annual Review of Fluid Mechanics*, 2007, 39: 89-106.
- Evangelio, A., Campo-Cortes, F., Gordillo, J. M. Simple and double microemulsions via the capillary breakup of highly stretched liquid jets. *Journal of Fluid Mechanics*, 2016, 804: 550-577.
- Gañán-Calvo, A. M. Generation of steady liquid microthreads and micron-sized monodisperse sprays in gas streams. *Physical Review Letters*, 1998, 80: 285-288.
- Guerrero, J., Chang, Y. W., Fragkopoulos, A. A., et al. Capillary-based microfluidics-coflow, flow-focusing, electro-coflow, drops, jets, and instabilities. *Small*, 2020, 16: 1904344.
- Montanero, J., Gañán-Calvo, A. M. Dripping, jetting and tip streaming. *Reports on Progress in Physics*, 2020, 83: 097001.
- Mu, K., Si, T., Ding, H. Nonlinear dynamics and manipulation of dripping in capillary flow focusing. *Science China-Physics Mechanics and Astronomy*, 2019, 62: 124713.
- Si, T., Li, F., Yin, X. Y., et al. Modes in flow focusing and instability of coaxial liquid-gas jets. *Journal of Fluid Mechanics*, 2009, 629: 1-23.
- Si, T., Li, F., Yin, X. Y., et al. Spatial instability of coflowing liquid-gas jets in capillary flow focusing. *Physics of Fluids*, 2010, 22: 112105.
- Sohrabi, S., Kassir, N., Moraveji, M. K. Droplet microfluidics: Fundamentals and its advanced applications. *RSC Advances*, 2020, 10: 27560-27574.
- Stone, H. A., Stroock, A. D., Ajdari, A. Engineering flows in small devices: Microfluidics toward a lab-on-a-chip. *Annual Review of Fluid Mechanics*, 2004, 36: 381-411.
- Zhu, A., Wang, L. Q. Passive and active droplet generation with microfluidics: A review. *Lab Chip*, 2017, 17: 34-75.